

# Onset and Growth of Adhesion Failure in Adhesively Bonded Tubular Socket joints in Laminated FRP Composites

Rashmi Ranjan Das<sup>1\*</sup> and Brajabandhu Pradhan<sup>1</sup>

<sup>1</sup> Department of Mechanical Engineering, Indian Institute of Technology, Kharagpur – 721 302, India

\*Corresponding author (email: [ra\\_swa@yahoo.com](mailto:ra_swa@yahoo.com), [rashmiranjandas@mech.iitkgp.ernet.in](mailto:rashmiranjandas@mech.iitkgp.ernet.in))

## Abstract

Finite element based simulation techniques for the analysis of adhesively bonded joints in tubular composite structures have been developed in the present research. Effective adhesive coupling length between the socket and the adherends for suitable performance of the Tubular Socket Joint (TSJ) is determined based on the Tsai-Wu failure criterion. Three-dimensional stress analyses revealed that peel stresses are more sensitive to three-dimensional effects than the shear stresses. Failure indices at different critical interfaces are evaluated using Quadratic Failure Criterion (QFC) within the adhesive and Tsai-wu coupled stress criterion for the adherend-adhesive and socket-adhesive interfaces. Based on the later criteria, locations prone to delamination damage (adhesion failure) initiation are identified to be existing at the interface of the loaded tubes and the adhesive, at the clamped edge side of the coupling length. Strain Energy Release Rate (SERR) calculated using Virtual Crack Closure Technique (VCCT) is used as the characterizing parameter for assessing the growth of delamination damage. Delamination damage propagation has been observed to be selfsimilar and it is found to propagate mainly in inplane shearing mode. As the damage propagates, its tendency towards opening mode of failure is decreased whereas it is increased in the inplane shearing mode. Unidirectionally fibre oriented adherends, especially GR/E [90]<sub>16</sub> are found to be more resistive to both the opening and inplane shearing mode growth of adhesion failure and hence are recommended as the best preferred fibre orientations for the bonded TSJ under tension to resist the adhesion failure. Increasing the degree of anisotropy of the composite adherends and socket improves the tendency of delamination damage growth resistance. B/E FRP composites are found to be the best among the various FRP composite adherend and socket combinations considered in the present study.

Keywords: Adhesion failure, Delamination damage, Failure index, FEM, QFC, SERR, Socket Joint, VCCT

## 1 Introduction

Fibre reinforced composite thin walled tubular structures have wide range of applications in aerospace, marine, chemical, petroleum and other industries for transportation of various fluids. Because of advantages like higher strength, leak proof and chemically inert smooth surface connections in harsh environments they have been used in piping systems for more than two decades. This application of composite materials was developed in response to significant corrosion problems associated with metallic pipes in the chemical processes in pulp and paper industries. Composite pipes have also been utilized in waste water treatment, power and petroleum productions. Most recently, composite tubes have been used in forming truss structures in space launch vehicles to reduce their weight. With properly developed manufacturing processes for composite pipes (such as centrifugal casting and computer controlled filament winding) within the past decade, the mechanical performances of such pipes have been dramatically improved. Ideally, a pipe system would be preferred to be designed without joints, since joints could be a source of weakness and / or excess weight. However, limitations on component size imposed by manufacturing processes and the requirement of inspection, accessibility, repair and transportation/ assembly necessitates some load carrying joints in most piping systems. The rule of thumb states that one joint should be installed for every four feet of composite pipe in marine applications, thus, further demanding the development of efficient composite pipe joints.

Bonded joints with tubular members under axial tension develop relatively high stresses with steep gradients localized at the joint ends. The stress concentrations which arise from geometric discontinuities are well established facts. In the event of failure, the process of delamination incipiates from these vulnerable and critical end-zones of the joints. One of the failure modes such as interlaminar or intralaminar delaminations, cohesion failure, adhesion failure or a combination thereof and their subsequent propagation/coalescence cause abrupt fracture in the adhesively bonded joints. Consequently, the importance of effective adhesive bonding has been recognized in the past years and considerable amounts of analytical, finite element and experimental works have been carried out on the subject of adhesive joints. A good amount of literature dealing with the stress analysis of adhesively bonded lap joints between flat adherends are available. However, literature

relating to bonded thin walled tubular lap joints are scanty.

The first paper treating the subject of tubular adhesive joints was published by Lubkin and Reissner [1]. They analyzed the stress distribution of the adhesive layer in tubular lap joints composed of thin walled circular cylindrical shell elements subjected to axisymmetric external loading. Among the investigations carried out on pipe joints, the problem of torsional stresses in tubular lap joint was first investigated by Volkersen [2]. In his analyses, two tubular adherends of the joint were treated by mechanics of materials approach, in which the presence of circumferential shear stress was ignored and the adhesive layer was treated as a sort of “shear spring” acting between two adherends. Following the work of Volkersen, Adams and Pepiatt [3] improved Volkersen’s analyses by taking into account the thickness of the adhesive layer. They also verified the basic results of Lubkin and Reissner. The stresses in two layered bonded orthotropic circular cylindrical shells were considered by Yucooglu and Updike [4]. Their analysis was based upon the assumption of axisymmetric external loading but with general condition for the principal direction of orthotropy. External bending and shear loading problems of tubular single lap joint (TSLJ) under non-axisymmetric loadings were also considered by Updike and Yucooglu [5], but along with the assumption of coincident direction of orthotropy and principal direction of curvature. Finite element based analyses of TSLJ composed of steel tube, adhesively bonded to a composite tube were done by Adams and Wake [6]. A two-dimensional polar theory for the analyses of the TSLJ by which the unknown parameters were related to composite layers was developed by Chon [7]. A variational principle of complementary energy method based stress distribution formulation for the adhesively bonded TSLJ under torsion was presented by Chen and Cheng [8]. A more general investigation for bonded laminated tubular joints was made by Thomsen [9] by considering that the principal direction of orthotropy does not have to coincide with the principal direction of curvature and loads are allowed to be non-axisymmetric type. More recently, Zou and Taheri [10] have investigated the response of various joint configurations subjected to torsion.

When the adherends are laminated FRP composites, they are vulnerable for various types of failures, viz. interlaminar failure and delaminations, etc., besides the conventional failures like cohesion and adhesion failures. Fracture mechanics parameters such as SERR, J-integral and SIF can be used to characterize the propagation of such failures or damages. Although a great deal of literature [11-16] is available for the damage prediction and its propagation in adhesively bonded flat laminated FRP composites, only a few have been devoted to the adhesively bonded TSLJ. Also, the literature contains very limited research on the calculation of SERR which is one of the key parameters for the study of adhesion or/and delamination damage propagation. Raju et al. [17] emphasized on SERR for the problem with skin stiffener debonding. The importance of SERR to characterize the delamination damages and their growths including the modelling aspects using Multi

Point Constraint (MPC) elements are discussed in detail by Pradhan and Chakraborty [18-19] and Pradhan and Panda [20].

Most of the analyses so far in this direction are of two-dimensional in nature considering flat adherends specifically with simplified assumptions which lacks explaining the mixed mode fracture behaviour of adhesively bonded joints of laminated FRP composites under general state of loading conditions. The present research is devoted to a simulation capability for the analysis of bonded joints in tubular structures using FEM consisting of layered brick elements for the adhesive and adherends. The effects of free rotation of the joint overlap and adherend have been considered. However, the secondary bending moment has been neglected. The objectives of this study are:

- (1) Determination of the effective coupling length of the socket and the adhesive to minimize the peak adhesive stresses
- (2) Identification of locations prone to delamination damage initiation in the joint
- (3) Study of adhesion failure propagation based on SERR computations
- (4) Study of the effect of ply-orientation and material anisotropy of the adherends on delamination damage propagation
- (5) Suitable design recommendations for improved joint performance

## 2 Finite element analysis of the TSJ

The geometry, configuration, loading and boundary conditions of the TSJ specimen analyzed is shown in Fig. 1. Two GR/E [0/90]<sub>s</sub> laminated FRP composite tubes are used as adherends and socket, whereas epoxy has been used as adhesive. The material properties along with their strength values for adhesive and adherends/socket are given in Table 1.

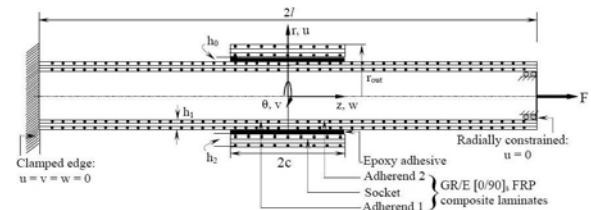


Fig. 1: Tubular socket joint (Sectional view).

The adhesive thickness ( $h_0 = 0.1$  mm), total length of the structure ( $2l = 178$  mm), outer radius of socket ( $r_{out} = 16$  mm), coupling thickness ( $h_2 = 1.5$  mm) and adherend thickness ( $h_1 = 1$  mm) are kept constant in the analysis. Whereas in search for an effective coupling length ( $2c$ ) to minimize the peak adhesive stresses, the coupling length has been varied in the range of 5mm to 36 mm.

Table 1. Material properties and strengths of the adherend/socket and adhesive.

Joint materials	Material constants	Strengths
-----------------	--------------------	-----------

T 300/934 graphite/epoxy FRP compo- site adherend/ socket	$E_z = 127.5$ GPa, $E_r = 4.8$ GPa $E_{\theta} = 9$ GPa	$Z_T = 1586$ MPa $Z_C = 1517$ MPa	
	$\nu_{zr} = \nu_{z\theta} = 0.28$ , $\nu_{\theta r} = 0.41$ $G_{zr} = G_{z\theta} = 4.8$ GPa $G_{\theta r} = 2.55$ GPa	$\theta_T = \theta_C = 80$ MPa $R_T = R_C = 49$ MPa $S = 2.55$ MPa	
Epoxy adhe- sive (isotropic)	$E = 2.8$ GPa, $\nu = 0.4$	$Y_T = 65$ MPa $Y_C = 84.5$ MPa	

Adhesive thickness ( $h_0 = 0.1$  mm) has been kept same from manufacturing point of view. The applied tensile load at the far end of the adherend 2 is equivalent to an uniform loading of intensity 10 MPa. Appropriate restrained boundary conditions have been taken for simulating pure axial loading in the TSJ. This is as follows:

- $u = v = w = 0$ , for all nodes along  $z = -l$ ; i.e. at the left end of the adherend 1, and
- $u = 0$ , for all nodes at  $r = \{r_{out} - (h_0 + h_1 + h_2)\}$  and  $z = +l$ ; i.e. near the loaded end of adherend 2.

where,  $u$ ,  $v$  and  $w$  represent the radial, circumferential and axial displacements associated with  $r$ ,  $\theta$  and  $z$  coordinates, respectively. The effects of free rotation of the joint overlap and adherend have been considered. However, the secondary bending moment has been neglected.

## 2.1 Finite element modelling

Finite element meshing of the TSJ specimen is shown in Fig. 2. Layered Solid 46 elements have been used to model the adherend composite and socket laminate ply-by-ply and orthotropic material properties have been inputted for each ply. The isotropic adhesive has been modelled using Solid 45 elements.

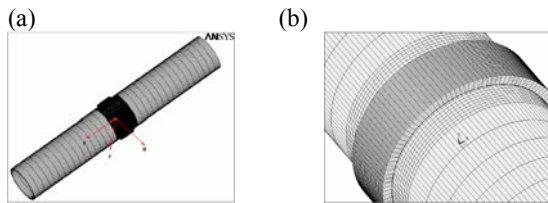


Fig. 2: Tubular socket joint with finite elements; (a) Full model and (b) Zoomed view of the overlap region.

## 3 Failure studies of the TSJ

The adhesively bonded socket joint experiences two important types of mechanical failures: (i) interfacial failure also known as adhesion failure which occurs between the adhesive and the adherends and (ii) cohesion failure within the adhesive apart from the failure or damage due to interlaminar delamination in the compo-

site adherends. Panigrahi and pradhan [11-16] have reported a detailed analysis of adhesion failure of bonded SLJ with flat adherends. The idea behind the current research is to understand the mechanics involved with the onset and growth of adhesion failure in boded TSJ.

### 3.1 Adhesion failure criterion

Using the out-of-plane stress values obtained from the three-dimensional stress analysis, which are responsible for the damages over different critical surfaces in the overlap region, the next step is to use these data to predict the location of damage initiation. Under the three-dimensional stress states in the overlap region, the adhesion failure at the interface of the adhesive and the adherend generally can be evaluated by the Tsai-Wu QFC [21] which takes into account the interaction of all six stress components given by:

$$\frac{\sigma_r^2}{R_T^2} + \frac{\sigma_\theta^2}{\theta_T^2} + \frac{\sigma_z^2}{Z_T^2} + \frac{\tau_{\theta r}^2}{S_{\theta r}^2} + \frac{\tau_{zr}^2}{S_{zr}^2} + \frac{\tau_{z\theta}^2}{S_{z\theta}^2} + \sigma_r \left( \frac{1}{R_T} - \frac{1}{R_C} \right) + \sigma_\theta \left( \frac{1}{\theta_T} - \frac{1}{\theta_C} \right) + \sigma_z \left( \frac{1}{Z_T} - \frac{1}{Z_C} \right) + f_{\theta r} \sigma_r \sigma_\theta + f_{zr} \sigma_z \sigma_r + f_{z\theta} \sigma_z \sigma_\theta = e^2 \quad (1)$$

where,  $R_T$ ,  $\theta_T$ ,  $Z_T$  are the allowable tensile strengths and  $R_C$ ,  $\theta_C$ ,  $Z_C$  are the allowable compressive strengths in the three principal material directions, respectively.  $S_{\theta r}$ ,  $S_{zr}$  and  $S_{z\theta}$  are the shearing strengths of the orthotropic layer in various coupling modes. The coupling coefficient reflecting the interaction between  $r$ ,  $\theta$  and  $z$  directions are given by  $f_{\theta r}$ ,  $f_{zr}$  and  $f_{z\theta}$ , respectively. Failure index ( $e$ ) is defined as the parameter to evaluate the condition whether the structure is likely to fail or not. If  $e \geq 1$  failure occurs, else there is no failure.

Generally, the interlaminar or out-of-plane stresses are responsible for the initiation of adhesion and delamination failures and hence only the interlaminar shear stresses ( $\tau_{\theta r}$  and  $\tau_{zr}$ ) and the through-the-thickness normal stress i.e. peel stress ( $\sigma_r$ ) are required to predict the damage initiation. Therefore, the Tasi-Wu criterion given in Eq. (1) reduces to the form as:

$$\left( \frac{\sigma_r}{R_T} \right)^2 + \left( \frac{\tau_{\theta r}}{S_{\theta r}} \right)^2 + \left( \frac{\tau_{zr}}{S_{zr}} \right)^2 = e^2 \begin{cases} e \geq 1, \text{ failure} \\ e < 1, \text{ no failure} \end{cases} \quad (2)$$

where,  $R_T$  is the interlaminar normal strength and  $S_{\theta r}$  and  $S_{zr}$  are the interlaminar shear strengths, respectively among the two orthogonal shear coupling directions. The FRP composite laminates considered in this research have  $S_{\theta r} = S_{zr}$ , because of material symmetry.

### 3.2 Cohesion failure criterion

The failure index of the TSJ in the adhesive layer is formulated by a cohesion failure philosophy. Following the parabolic yield criterion for isotropic materials pro-

posed by Raghava et al. [22], the identification of location of cohesion failure initiation in the adhesively bonded tubular lap joint can be made. The criterion is given by:

$$(\sigma_1 - \sigma_2)^2 + (\sigma_2 - \sigma_3)^2 + (\sigma_3 - \sigma_1)^2 + 2(|Y_C| - Y_T)(\sigma_1 + \sigma_2 + \sigma_3) = 2Y_C|Y_T|e \quad (3)$$

where,  $\sigma_1$ ,  $\sigma_2$  and  $\sigma_3$  are the principal stresses in the isotropic adhesive material causing yield and  $Y_C$  and  $Y_T$  are the absolute values of the compressive and tensile yield strengths, respectively. It may be noted that when  $Y_C$  and  $Y_T$  are equal, the above yield criterion reduces to the most familiar von-Mises yield criterion.

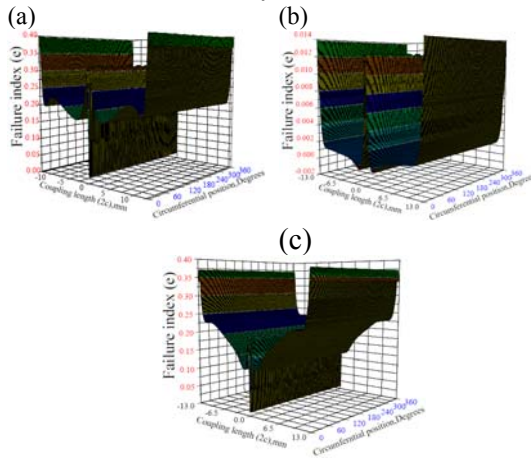


Fig. 3: Distribution of failure indices: (a) at the interface of adherend and adhesive (b) at the mid surface of adhesive layer, and (c) at the interface of socket and adhesive. (for coupling length  $2c = 26\text{mm}$ ).

Using Eqs. (1) - (3) with material properties given in Table 1, the failure indices are calculated at three critical interfaces over the coupling length and are shown in Fig. 3 for an overlap length of  $2c = 26\text{mm}$ . It is clearly observed that failure index attains a maximum value at the inner adherend-adhesive interface near the edge of the overlap length closer to the clamped end of the TSJ. Hence, this is the location which is more prone to adhesion failure initiation.

#### 4 Effective overlap length of the TSJ

Coupling length is one of the key geometrical parameters influencing stress distribution within the adhesive and the adjoining FRP composite adherends and socket. In search of determining a suitable coupling length to obtain favourable stress distributions, the coupling length has been varied in the range of 5mm to 36 mm, with an adhesive thickness of 0.1mm. For each coupling length, the Tsai-Wu criterion (Eq. (2)) is applied at the interface of adherends and adhesive to assess the failure index ( $e$ ). These are shown in Fig. 4.

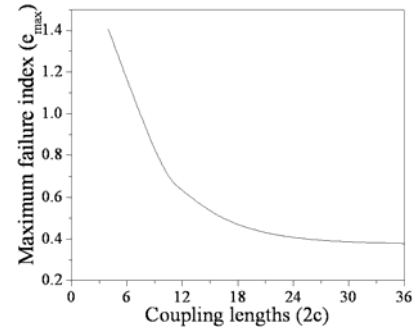


Fig. 4: Variation of max. failure index ( $e_{\max}$ ) for different coupling lengths.

The overlap lengths in the range  $0 < 2c \leq 7\text{mm}$  are not accepted, since  $e \geq 1$ . Though the failure indices for all overlap length values greater than 26 mm are well within the limit, there is no reason to adopt overlap length  $2c \geq 26\text{mm}$  since this would unnecessarily occupy extra space and add on to the weight of the structure. The working range of the coupling length, therefore, should be  $7\text{mm} \leq 2c \leq 26\text{mm}$ . Here-in-after an overlap length ( $2c$ ) of 26 mm would be adopted for the TSJ under consideration.

### 5 Adhesion failure of the TSJ

The damage analysis is now performed for the TSJ specimen by simulating an embedded adhesion failure at the interface of the inner adherend and adhesive close to the clamped end of the TSJ.

Adhesion failure of length ' $a$ ' is considered to be present at the interface of the loaded adherends and adhesive towards the clamped edge of the structure. MPC elements are used along the delamination damage front to extract the nodal forces responsible to close the damage. The damage analysis is now performed for the TSJ specimen by simulating an embedded adhesion failure at the interface of the inner adherend and adhesive close to the clamped end of the TSJ.

#### 5.1 Computations of SERR

Adhesion failure of length ' $a$ ' is considered to be present at the interface of the loaded inner adherend and adhesive towards the clamped edge of the structure. MPC elements are used along the delamination damage front to extract the nodal forces responsible to close the damage.

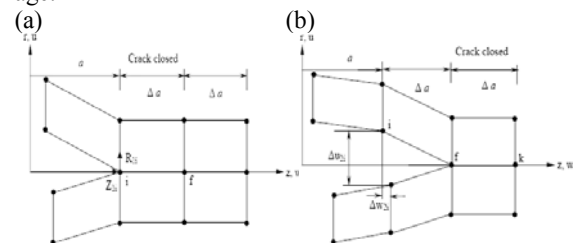


Fig. 5: Two-dimensional crack closure method: (a) First step: crack closed and (b) Second step: crack extended.

These nodal forces are useful for the calculation of SERR using the VCCT. The VCCT is based upon the same assumptions as Irwin's crack closure integral method [23]. The MCCI developed by Irwin and used by Rybicki and Kanninen [24] is used in the present analysis for calculation of the components of SERR. The method is based on the assumption that the energy  $\Delta E$  released when the crack is extended by ' $\Delta a$ ' from ' $a$ ' (Fig. 5(a)) to ' $a + \Delta a$ ' (Fig. 5(b)) is identical to the energy required to close the crack between locations  $i$  and  $f$ . For a crack modelled with two-dimensional four-noded elements as shown in Fig. 5. the work  $\Delta E$  required to close the crack along one element side can be calculated as:

$$\Delta E = \frac{1}{2} (Z_{1i} \cdot \Delta w_{2i} + R_{1i} \cdot \Delta u_{2i}) \quad (4)$$

where  $Z_{1i}$  and  $R_{1i}$  are the inplane shear and radial opening forces at nodal point  $i$  to be closed (Fig. 5(a)) and  $\Delta w_{2i}$  and  $\Delta u_{2i}$  are the differences in shear and opening nodal displacements at node  $i$  as shown in Fig. 5(b).

This method establishes the original condition before the crack was extended. Therefore, the forces required to close the cracks are identical to the forces acting on the upper and lower surfaces of the closed crack. The forces  $Z_{1i}$  and  $R_{1i}$  may be obtained from a first finite element analysis where the crack is closed as shown in Fig. 5(a). The displacements  $\Delta w_{2i}$  and  $\Delta u_{2i}$  are obtained from a second finite element analysis where the crack has been extended to length ' $a + \Delta a$ ' as in Fig. 5(b). Additionally, it is assumed that a crack extension of ' $\Delta a$ ' from ' $a + \Delta a$ ' (node  $f$ ) to ' $a + 2 \Delta a$ ' (node  $k$ ) does not significantly alter the state at the crack tip. Therefore, the displacements behind the crack tip at node  $f$  are approximately equal to the displacements behind the original crack tip at node  $i$ . Further, the energy  $\Delta E$  released when the crack is extended by ' $\Delta a$ ' from ' $a + \Delta a$ ' to ' $a + 2 \Delta a$ ' is identical to the energy required to close the crack between locations  $f$  and  $k$ . Thus, the work required to close the crack along one element side can be calculated using Eq. (4). The forces and displacements required to calculate the energy  $\Delta E$  to close the crack may be obtained from one single finite element run.

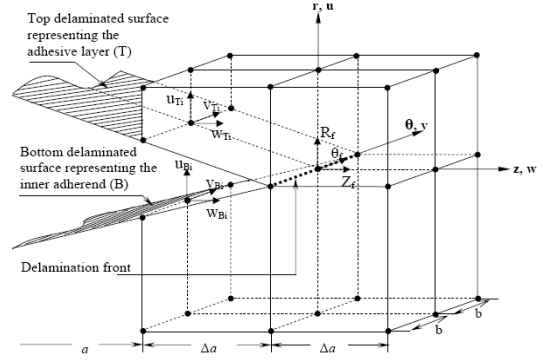


Fig. 6: VCCT for the damage study in TSJ with eight noded solid elements

A portion of the TSJ specimen with adhesion failure is shown in Fig. 6 along with the finite element mesh consisting of one layer of eight noded three-dimensional solid elements representing the inner adherend and the adhesive layer. In the present study, the adhesion failure is considered as a typical delamination damage existing at the interface of the inner adherend and the adhesive layer. The length of the delamination is taken as ' $a$ ' and is represented as a two-dimensional discontinuity by two surfaces. The additional dimension allows calculating the distribution of the energy release rates along the delamination front and making it possible to obtain  $G_{III}$ , which is identical to zero for two-dimensional models. Nodes at the top and bottom surfaces of the delaminated area have identical coordinates and are not connected with each other. The delamination front is represented by two rows of nodes coupled through the MPC elements (MPC 184). The undamaged section where the joint is intact is modelled using single nodes. Referring to Fig. 6, the mode I, mode II, and mode III components of strain energy release rates  $G_I$ ,  $G_{II}$  and  $G_{III}$  at point  $f$  in the delamination front are calculated as:

$$G_I = \frac{1}{2\Delta A} R_f (u_{Ti} - u_{Bi}) \quad (5)$$

$$G_{II} = \frac{1}{2\Delta A} Z_f (w_{Ti} - w_{Bi}) \quad (6)$$

$$G_{III} = \frac{1}{2\Delta A} \theta_f (v_{Ti} - v_{Bi}) \quad (7)$$

where,  $\Delta A = (\Delta a \cdot b)$  is the area virtually closed. ' $\Delta a$ ' is the length of the element at the delamination front and ' $b$ ' is the width of the elements.  $R_f$ ,  $Z_f$  and  $\theta_f$  denote the forces in the delamination front at the node  $f$  and the corresponding displacements behind the delamination front at the top delaminated surface representing the adhesive layer (T) nodes are denoted by  $u_{Ti}$ ,  $v_{Ti}$  and  $w_{Ti}$  and at the bottom delaminated surface representing the inner adherend (B) nodes are denoted by  $u_{Bi}$ ,  $v_{Bi}$  and  $w_{Bi}$ . All forces and displacements are obtained from fi-

nite element analysis with respect to global coordinate system. Using Eqs. (5) - (7) the SERRs  $G_I$ ,  $G_{II}$  and  $G_{III}$  are calculated for different delamination lengths.

## 6 Results and discussions

### 6.1 Stress analysis

Three-dimensional effects are observed in the out-of-plane shear stress distributions. However, ' $\tau_{\theta r}$ ' is more sensitive to the three-dimensional effect compared to other stresses ( $\sigma_r$  and  $\tau_{zr}$ ). These observations for the TSJ are similar to the observations of Panigarhi and Pradhan [11] for the SLJ. It is interesting to note that the peel stress at the interface of adherends and adhesive attains maximum value as compared to the other two critical regions. Further, it may be observed that the peel stress is larger towards the clamped end side of the overlap length than the loaded end side at the adherend-adhesive interface. Similar trend is also observed with the out-of-plane shear stress ( $\tau_{zr}$ ).

### 6.2 Joint strength characteristics

The stress analysis reveals that the location of the failure initiation can not be predicted with full conviction. There are three surfaces which are critical for the initiation of failure. They are (i) adherend-adhesive interface (ii) socket-adhesive interface and (iii) mid-surface of the adhesive layer. Using Eqs. (2) and (3), failure indices ( $e$ ) have been calculated for the adherend-adhesive and socket-adhesive interfaces and the mid-surface of the adhesive layer, respectively. The distributions of failure indices over the critical surfaces as shown in Fig. 5, indicate that the possibility of failure initiation would be from the interface of inner adherends and adhesive near the edge of the overlap length closer to the clamped end side of the TSJ. The value of failure index ' $e$ ' is maximum here as compared to the other locations.

### 6.3 Delamination damage characteristics

Fig. 7 illustrates the distribution of SERRs i.e.  $G_I$ ,  $G_{II}$  and  $G_{III}$ ; in mode I, mode II and mode III along the circumferential delamination damage front, with a simulated delamination length,  $a = 2$ mm.

This indicates a selfsimilar growth of the delamination damage in the TSJ under tension; unlike in bonded SLJ where damage propagates in a non-self similar manner as reported by Panigarhi and Pradhan [11] in their study for the SLJ. Magnitudes of SERRs reveal that the inplane shearing mode ( $G_{II}$ ) is dominant whereas the out-of-plane shearing mode ( $G_{III}$ ) is meager.

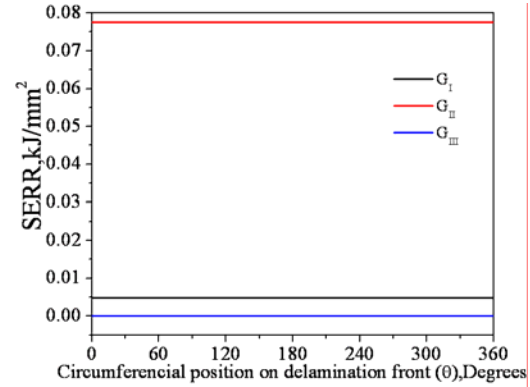


Fig. 7: Variation of different modes of SERR along the circumference of the delamination front of length  $a = 2$  mm.

As the damage propagates, its tendency towards opening mode of failure is reduced whereas it tends more towards an inplane shearing mode of failure (Fig. 8). Mode-II ( $G_{II}$ ) is more responsible for the propagation of the damage due to adhesion failure. This explains the fact that adhesively bonded socket joints experience predominantly a shearing failure.

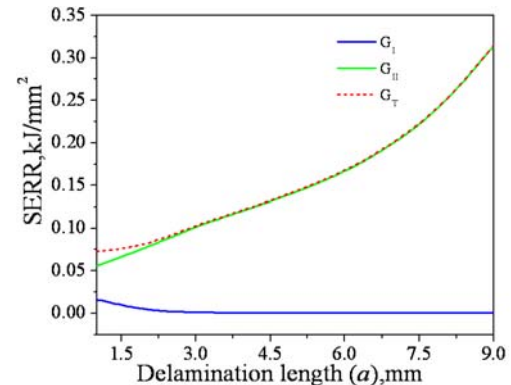
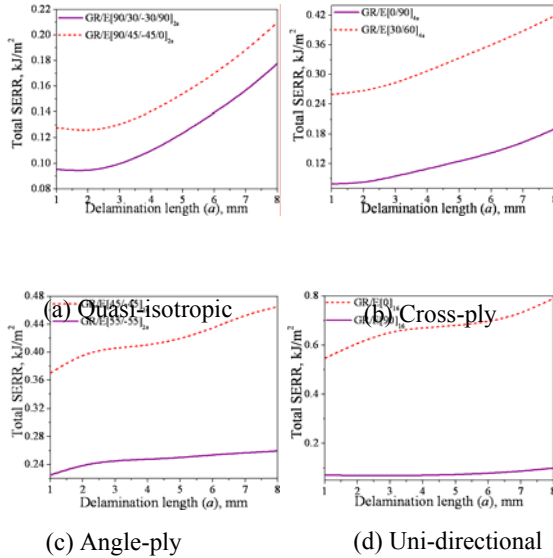


Fig. 8: Variation of different modes of SERR with changing delamination lengths of adhesion failure

### 6.4 Effect of ply-orientation on delamination damage growth

To assess the effect of different ply-orientations of the laminates on the propagation of the adhesion failure in the TSJ subjected to an uniaxial tensile loading, eight different ply configurations were considered and the unidirectional prepregs were laid up in quasi-isotropic ( $[90/\pm 45/0]_{2s}$  and  $[90/\pm 30/90]_{2s}$ ), cross-ply ( $[0/90]_{4s}$  and  $[30/60]_{4s}$ ), angle-ply ( $[45/-45]_{4s}$  and  $[55/-55]_{4s}$ ) and unidirectional ( $[0]_{16}$  and  $[90]_{16}$ ) orientations. Fig. 9 demonstrates the effect of these ply-orientations on total SERR ( $G_T$ ).



**Fig. 9:** Effect of stacking sequence on total SERR  $G_{III}$ , during delamination damage propagation in various types of adherend and socket laminates. Considering the total SERR  $G_T$  as a prominent parameter, it is evident from Fig. 9 that plies oriented unidirectionally in the direction of the applied load i.e.  $[90]_{16}$  are the most preferred orientations, especially for the TSJ under uniaxial loading.

### 6.5 Effect of adherend anisotropy on delamination damage growth

Keeping the ply-orientation as  $[90]_{16}$ , the constituent materials of the adherends and the socket are now considered to be GL/E, C/E and B/E in order to examine the effect of adherend anisotropy on the damage propagation (Fig. 10).

It is observed that as the degree of anisotropy is increased in the above stated order, the tendency of the growth of delamination damage reduces. The B/E FRP composite laminated adherends are found to be the best in regards to the delamination damage growth resistance.

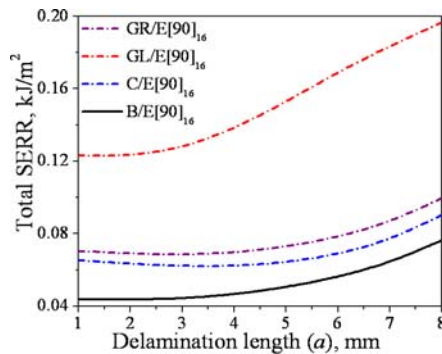


**Fig. 10:** Effect of adherend and socket anisotropy on total SERR during delamination damage propagation.

## 7 Conclusions

Some of the salient conclusions drawn from the present analysis are as follows:

- Analytical solutions for the damage study of the TSJ of laminated FRP composites exist for simple geometry, loading and boundary conditions. In real applications of bonded joints involving complicated geometry, loading and boundary conditions, three-dimensional finite element analyses are essential to model all types of damage problems of bonded joints.
- For effective performance of the TSJ, effective adhesive coupling length between the socket and the adherends is recommended to be between 7mm to 26mm.
- Delamination damage (adhesion failure) initiates at the edge of the adherend-adhesive interface of the coupling length close to the clamped end side of the TSJ.
- The delamination damage in the TSJ propagates in a selfsimilar manner unlike that in the SLJ with flat FRP composite adherends.
- The delamination damage propagates mainly in inplane shearing mode, as compared to opening or tearing modes. As the delamination damage propagates, its tendency towards opening mode of failure is reduced whereas it is more prone to delaminate in the inplane shearing mode.
- Plies oriented in the direction of applied load (especially  $[90]_{16}$ ) are the most preferred orientations for the bonded TSJ under tension to resist the adhesion failure.
- Increasing the degree of anisotropy of the adherends reduces the tendency of delamination damage growth. The B/E FRP composite adherends are found to be the best as compared to GL/E, C/E and GR/E FRP composite laminates considered in the present study.

## References

- [1] J.L. Lubkin and E. Reissner, "Stress Distribution and Design Data for Adhesive Lap Joints between Circular Tubes," *Journal of Applied Mechanics*, Vol. 78, 1958, pp. 1213-1221.
- [2] O. Volkersen, Recherches Sur la Théorie des Assemblages Colles, *Construction Métallique*, Vol. 4, 1965, pp. 3-13.

- [3] R.D. Adams and N.A. Peppiatt, "Stress Analysis of Adhesive Bonded Lap Joints," *Journal of Adhesion*, Vol. 9, 1977, pp. 1-18.
- [4] U. Yuceoglu and D.P. Updike, "Stresses in Two-Layer Bonded Orthotropic Cylindrical Shells," *Emerging Technologies in Aerospace Structures, Design, Structural Dynamics and Materials*. ASME, New York, 1980, pp. 53-65.
- [5] D.P. Updike and U. Yuceoglu, "Tubular Lap Joints in Composite Cylindrical Shells under External Bending and Shear," *Progress in Science and Engineering Composites, ICCM-IV, Tokyo*, 1982, pp. 297-304.
- [6] R.D. Adams and W.C. Wake, "Structural Adhesive Joints in Engineering," *London: Elsevier Applied Science*, 1984.
- [7] T.C. Chon, "Analysis of Tubular Lap Joint in Torsion," *Journal of Composite Materials*, Vol. 16, 1982, pp. 268-284.
- [8] D. Chen and S. Cheng, "Torsional Stress in Tubular Lap Joints," *International Journal of Solid and Structures*, Vol. 29, 1992, pp. 845-853.
- [9] O.T. Thomsen, "Elasto-static and Elasto-plastic Stress Analysis of Adhesive Bonded Tubular Lap Joints," *Composite Structures*, Vol. 21, 1992, pp. 249-259.
- [10] G.P. Zou and F. Taheri, "Stress Analysis of Adhesively Bonded Sandwich Pipe Joints Subjected to Torsional loading," *International Journal of Solids and Structures*, Vol. 43, 2006, pp. 5953-5968.
- [11] S.K. Panigrahi and B. Pradhan, "Three Dimensional Failure Analyses and Damage Propagation Behaviour of Adhesively Bonded Single Lap Joints in Laminated FRP Composites," *Journal of Reinforced Plastics and Composites*, Vol. 26, 2007, pp. 183-201.
- [12] S.K. Panigrahi and B. Pradhan, "Adhesion Failure Propagation in Adhesively Bonded Single Lap Laminated FRP Composite Joints," *Journal of Adhesion Science and Technology*, Vol. 21, 2007, pp. 379-398.
- [13] S.K. Panigrahi and B. Pradhan, "Delamination Damage Analyses of Adhesively Bonded Lap Shear Joints in Laminated FRP Composites," *International Journal of Fracture*, Vol.148, 2007, pp. 373-385.
- [14] S.K. Panigrahi and B. Pradhan, "Delamination Damage Analyses of FRP Composite Spar Wingskin Joint with Modified Elliptical Adhesive Load Coupler Profiles," *Applied Composite Materials*, Vol. 15, 2008, pp.189-205.
- [15] S.K. Panigrahi and B. Pradhan, "Onset and Growth of Adhesion Failure and Delamination Induced Damages in Double Lap Joint of Laminated FRP Composites," *Composite Structures*, Vol. 85, 2008, pp. 326-336.
- [16] S.K. Panigrahi and B. Pradhan, "Through-the-Width Delamination Damage Propagation Characteristics in Single Lap Laminated FRP Composite Joints," *International Journal of Adhesion and Adhesives*, Vol. 29, 2009, pp. 114-124.
- [17] I.S. Raju, R. Sistla and T. Krishnamurthy, "Fracture Mechanics Analysis of Skin-Stiffener Debonding," *Engineering Fracture Mechanics*, Vol. 54(1), 1996, pp. 371-385.
- [18] B. Pradhan and D. Chakraborty, "Fracture Behaviour of FRP Composite Laminates with Embedded Elliptical Delaminations at the Interface," *Journal of Reinforced Plastics and Composites*, Vol. 19(13), 2000, pp. 1004-1023.
- [19] B. Pradhan and D. Chakraborty, "Effect of Ply Thickness and Fibre Orientation on Delamination Initiation in Broken Ply Composites," *Journal of Reinforced Plastics and Composites*, Vol. 18(8), 1999, pp. 735-757.
- [20] B. Pradhan and S.K. Panda, "The Influence of Ply Sequence and Thermoelastic Stress Field on Asymmetric Delamination Crack Growth Behaviour of Embedded Elliptical Delaminations in Laminated FRP Composites," *Composite Science and Technology*, Vol. 36(3-4), 2006, pp. 1004-1023.
- [21] S. W. Tsai and E. M. Wu, "A General Theory of Strength for Anisotropic Materials," *Journal of Composite Materials*, Vol. 5, 1971, pp. 58-80.
- [22] R. S. Raghava, R. M. Cadell and G. S. Yeh, "The Macroscopic Yield Behaviour of Polymers," *Journal of Material Science*, Vol. 8, 1973, pp. 225-232.
- [23] G. R. Irwin, "Analysis of Stresses and Strains Near the End of a Crack Traversing a Plate," *ASME Trans., Journal of Applied Mechanics*, Vol. 24, 1957, pp. 361-364.
- [24] E. F. Rybicki and M. F. Kanninen, "A Finite Element Calculation of Stress Intensity Factors by a Modified Crack Closure Integral," *Engineering Fracture Mechanics*, Vol. 9, 1977, pp. 931-938.